Self-consistent spline augmented-plane-wave calculation: Ground-state properties of Cu

G. M. Fehrenbach and H. Bross
Sektion Physik der Ludwig Maximilians Universität München, Theresienstraße 37, 80333 Munich, Federal Republic of Germany
(Received 2 August 1993)

The self-consistent generalization of the spline augmented-plane-wave method within a full-potential density-functional framework is presented. The band-structure scheme properly accounts for the **k**-dependent split-up of the radial wave functions R_l into R_{lm} in the case of an arbitrary potential. As an application we investigate ground-state and related properties of bulk Cu. Full-potential effects turn out to play a minor role. Surprisingly, the absolute value of the equilibrium total energy is found 1.305 Ry below the former result of Moruzzi *et al.*, although the same exchange-correlation potential is employed. The calculated equilibrium values of the lattice constant, bulk modulus, and form factors agree quite satisfactorily with experimental results, while the band energies characteristically deviate from photoemission data. Whenever possible, we compare our results to experimental and previous theoretical data.

I. INTRODUCTION

Full-potential, linear, all-electron calculations within the local-spin-density approximation (LDA) on the density-functional formalism[1] have contributed essentially to the microscopic understanding of crystalline solids. Calculations of the ground-state properties based on modified augmented-plane-wave[2–4] (MAPW), on linear combination of Gaussian orbitals[5] (LCGO), or full-potential linearized-augmented-plane-wave[6–9] (FLAPW) band-structure schemes are commonly believed to be very accurate.

Although these (and other) schemes are successful, recent discoveries show that significant problems remain: (i) The so-called extended core-state problem[10,11] in current FLAPW investigations, which is a consequence of the nonorthogonality[10,11] that occurs generally within this scheme. (ii) The incompleteness of the finite-basis set in any calculation scheme. This was shown to reduce the numerical accuracy in current calculations of the dielectric matrix.[12,13] (iii) Furthermore, many full-potential methods, e.g., FLAPW, treat the nonspherical potential only by including matrix elements underlying the solution of the Schrödinger equation for the spherical part of the potential.

The origin and the consequences of these failures can be divided into logically different contributions. (i) The nonorthogonality of states (e.g., in LAPW) occurs usually because energy derivative techniques are used to linearize the secular equation, with the outcome that states are no longer orthogonal to each other if they belong to different energy windows. This might cause an unphysical lowering of the eigenvalues as well as artifacts in the charge density.[11] (ii) The incompleteness of the finite numerical basis set becomes important if infinite sums are involved.[12] For their evaluation, the number of valence and conducting bands which can be obtained is often too small to ensure convergence. For linear schemes the number of bands is, in turn, limited by the rank of the secular equation. Therefore, it becomes important to linearize the band-structure problem over a large energy range.[14] (iii) A nonspherical potential in the muffin-tin spheres is inevitably difficult to treat exactly. In principle, it requires the solution of an infinite set of differential equations[15] for the radial functions R_{lm} or, equivalently, a solution of a Volterra-type integral equation.[16,17] This has up to now never been employed in an APW-like framework.

In a previous paper[14] the authors proposed the spline augmented-plane-wave method (SAPW), which has a basis that numerically forms a complete set with respect to the important (but here cumbersome) operator of momentum to any accuracy desired. This method consists of an expansion of the R_{lm} into cubic B splines,[18] one form of the one-dimensional finite element method,[19] which is among the most powerful techniques of numerical analysis: On the one hand it makes the computations as simple as possible, on the other hand it enables direct estimations of the accuracy of the final Ritz procedure.[14,19] Also the orthonormality of the wave functions is precisely ensured.

In the present paper we continue this work attaining the self-consistent generalization of Ref. 14, and turn our attention on the influence of the shape of the effective one-electron potential. After a brief review of the SAPW method, which introduces our notation, the theory of our self-consistent procedure is outlined in Sec. II. In Sec. III we present our numerical results for Cu. First of all, we analyze the magnitude of full-potential effects and the split-up of the R_l into R_{lm}. Secondly, we analyze the ground-state properties under uniform pressure and compare the LDA eigenvalues to photoemission data. We close by discussing our results in Sec. IV. Details of the generalized Ewald technique to calculate the electrostatic potential of the proton and multipole lattice are given in the Appendix.

II. THE CALCULATION SCHEME

A. The band structure

We divide the elementary cell Ω into M nonoverlapping spheres $\mathcal{H}_\mu$ with radius s_μ centered at the atomic sties $\mathbf{R}_\mu$ and into the remaining interstitial region $\mathcal{I}$. Restricting ourselves to the paramagnetic case we write the Ritz-Galerkin SAPW ansatz in the central Wigner Seitz cell[14]

 ©1993 The American Physical Society

$$\Psi_{n\mathbf{k}}(\mathbf{r})=\sum_{\mathbf{k}_j\le q} A_j^{(1)}\exp(i\mathbf{k}_j\cdot\mathbf{r})+\exp(i\mathbf{k}\cdot\mathbf{R}_\mu)\sum_{\mu=1}^{M}\sum_{L\le\lambda_\mu}\sum_{s=1}^{N_\mu(l)} A_{\mu Ls}^{(2)}Y_L(\hat{\mathbf{t}}_\mu)(it_\mu)^l B_{sl}(t_\mu)\ , \tag{1}$$

with the usual notations $\mathbf{k}_j=\mathbf{k}+\mathbf{G}_j$ and $\mathbf{t}_\mu=(\mathbf{r}-\mathbf{R}_\mu)/s_\mu$, where $t_\mu\le 1$. $Y_L(\hat{\mathbf{t}}_\mu)$ is a real valued spherical harmonic, $L=(l,m)$ an angular momentum multiindex, and $L\le\lambda$ stands for all pairs (l,m) with $l\le\lambda$. Outside the first cell $\Psi_{n\mathbf{k}}(\mathbf{r})$ is continued according to Bloch's boundary condition.

So far the idea is an old one. What is new is the choice of the trial functions $B_{sl}(t)$: We defined[14] them on a radial grid, which in numerical calculations is the one first introduced by Moruzzi, Janak, and Williams[20]

$$\mathcal{G}_N=\left\{t^{(0)},\ldots,t^{(N)}\ \middle|\ \text{with } t^{(i)}=\left[\frac{i}{N}\right]^2\right\} \tag{2}$$

as polynomials of third order pieced together with continuous second derivative on each point of the partition (2). In addition, these B_{sl} fulfill the boundary condition

$$B_{sl}(t)=B'_{sl}(t)=0\quad\text{for all } s=0,\ldots,N_\mu(l) \tag{3}$$

and $t\ge 1$, so that the first derivative of $\Psi_{n\mathbf{k}}$ will become continuous. By construction, each B_{sl} is zero over most of the domain [0,1] and enters the computation only in the neighborhood of $t^{(s)}$. Usually, these functions are referred to as B splines[18] or one-dimensional finite elements.[19] In order to satisfy the boundary condition (3) we defined a special basis of B splines consisting of as many functions as there are points in the grid (2). This set is used in the ansatz (1), and discussed in detail and illustrated in Ref. 14.

The variational parameters $A^{(1)}$ and $A^{(2)}$ of the ansatz (1) are evaluated by a linear, Hermitian eigenvalue problem of the general type

$$[\underline{H}_{\mathbf{k}}-E_{n\mathbf{k}}\underline{O}_{\mathbf{k}}]\underline{A}_{n\mathbf{k}}=0\ , \tag{4}$$

where $\underline{H}$ and $\underline{O}$ are the matrices of the Hamiltonian and the overlap, respectively, and the coefficients $A^{(1)}$ and $A^{(2)}$ of (1) are arranged linearly in the array $\underline{A}$. The rank N of the problem (4) is given by

$$N=P+\sum_{\mu}^{M}\sum_{l=0}^{\lambda_\mu}(2l+1)N_\mu(l)\ , \tag{5}$$

with the number of plane waves P. Generally, the N_μ which define the radial discretizations were chosen to be powers of 2, and a reasonable lower limit is 16 if the shell is occupied in the corresponding atom. In our numerical investigations in Sec. III, N will take values of about 500 while additional calculations were performed in the case of Si and Ge with $N>1000$, reflecting that this method needs the capabilities of large computers. The details, the resulting properties, and the accuracy of the SAPW method are discussed exhaustively in Ref. 14 and we only summarize the most important of them here.

(i) Because the scheme is strictly linear, all states are mutually orthogonal within the accuracy of the computer.

(ii) The matrix elements of the Hamiltonian and the overlap can be calculated analytically (Appendix A of Ref. 14).

(iii) To any accuracy desired, the ansatz (1) forms a complete set with respect to the momentum operator, provided that the parameters $[q,\lambda_\mu,N_\mu(l)]$ are suitably chosen.

(iv) The error of the radial parts of the wave function decreases pointwise like $(t^{(i+1)}-t^{(i)})^4$ with an increasing number of B splines.

Using the ansatz (1), the shape of the potential in $\mathcal{J}$ cannot be subject to any restriction of practical use, because it enters the calculation only by its Fourier coefficient.[14] In each $\mathcal{H}_\mu$ we assume that the potential can be approximated properly by the finite multipole series

$$V(\mathbf{r})\approx\sum_{L\le l_p} Y_L(\hat{\mathbf{t}}_\mu)V_L(t_\mu)\quad\text{for all } \mathbf{r}\in\mathcal{H}_\mu \tag{6}$$

truncated after $L=l_p$.

From the ansatz (1) we observe that the radial behavior of $\Psi_{n\mathbf{k}}$ in $\mathcal{H}_\mu$ is described by a superposition of the following two terms:

$$R_{L\mu}^{(1)}(t_\mu)=4\pi i^l\sum_j \exp(i\mathbf{k}_j\cdot\mathbf{R}_\mu)A_j^{(1)}Y_L(\hat{\mathbf{k}}_j)j_l(k_j s_\mu t_\mu)\ , \tag{7}$$

$$R_{L\mu}^{(2)}(t_\mu)=(t_\mu i)^l\exp(i\mathbf{k}\cdot\mathbf{R}_\mu)\sum_s A_{sL\mu}^{(2)}B_{sl}(t_\mu)\ , \tag{8}$$

with the spherical Bessel function j_l. The first contribution (7) arises from the plane-wave part in the ansatz, ensures Bloch's boundary condition, and is solely responsible for the behavior of $\Psi_{n\mathbf{k}}$ if $L>\lambda_\mu$. Corresponding to the upper limit l_p in (6) the terms with $L>\lambda_\mu+l_p$ in (7) do not contribute to the potential energy in $\mathcal{H}_\mu$. Above that, the second contribution (8) describes the oscillating behavior near the nucleus μ and since the parameters $A_{sL\mu}^{(2)}=A_{s(l,m)\mu}^{(2)}$ are estimated independently by the variational procedure for different values of m the radial behavior (8) varies with m. By this variational solution we avoid the difficulties connected with the coupled differential equations. Furthermore, this technique enables us to investigate the m dependence of the radial behavior of $\Psi_{n\mathbf{k}}$ and compare it with the results of the en-

ergy derivative technique.[6,7]

Closing this summary we point out that the augmentation scheme of the SAPW ansatz (1) is closely related but even more lucid than the one used in MAPW (Ref. 2) which, in turn, benefits from the smaller rank of its eigenvalue problem. However, both significantly deviate from several techniques used in (F)LAPW (Refs. 6 and 7) and their extensions[11,21] by the fact that the plane-wave part is found also inside the spheres $\mathcal{K}_\mu$.

B. Electron density

The density of electrons can be written in the form

$$\rho(\mathbf{r})=\sum_{G_j\le G_{\max}}\rho^{(1)}_{\mathbf{G}_j}\exp(i\mathbf{G}_j\cdot\mathbf{r}) + \sum_{\mu=1}^{M}\sum_{L\le\infty} t^l_\mu P_{L\mu}(t_\mu)Y_L(\hat{\mathbf{t}}_\mu) \tag{9}$$

as superposition of a plane wave and a localized part with

$$\rho^{(1)}_{\mathbf{G}_j}=\frac{2\Omega}{(2\pi)^3}\sum_n\int_{E_{n\mathbf{k}}\le E_F}d^3k\sum_{\mathbf{k}_{j'}\le q}A^{(1)}_{j'}A^{(1)*}_{j'-j}\ , \tag{10}$$

$$t^l_\mu P_{L\mu}(t_\mu)=\sum_{L'\le\lambda_\mu}\sum_{L''\le\lambda_\mu+l}C^L_{L',L''}\frac{2\Omega}{(2\pi)^3}\sum_n\int_{E_{n\mathbf{k}}\le E_F}d^3k\{R^{(2)}_{L'\mu}(t_\mu)R^{(2)*}_{L''\mu}(t_\mu)+2\mathrm{Re}[R^{(2)}_{L'\mu}(t_\mu)R^{(1)*}_{L''\mu}(t_\mu)]\}\ . \tag{11}$$

Here $C^L_{L',L''}=\langle L'|L|L''\rangle$ denotes the Gaunt coefficient[22] with the real valued spherical harmonics and E_F is the Fermi energy. As a consequence of the boundary conditions (3) the multipole contributions (11) vanish including their first derivatives at the boundaries $t_\mu=1$ of every sphere $\mathcal{K}_\mu$ and outside of them. It is worth noting that (11) gives not only the complete charge in the spheres but each term $\rho^{(1)}_{\mathbf{G}_j}$ contributes, also. In the same manner as for the $\Psi_{n\mathbf{k}}$ in (1) the density of electrons (9) consists of a finite number of Fourier terms and a localized part with the continuous first derivative everywhere vanishing outside of all spheres. Independently of the ansatz parameter λ_μ, the multipole expansion of the localized part does not truncate.

Closely related to the choice of trial functions B_{sl} the $P_{L\mu}$ are expressed by their spline interpolation

$$P_{L\mu}(t)=\sum_{j=0}^{3}\mathrm{P}^{(i,j)}_{L\mu}t^j \quad \text{for } t^{(i-1)}\le t\le t^{(i)} \tag{12}$$

in numerical calculations on the grid (2) with $N=512$ points. In the remainder (12) enables us to evaluate all radial integrals analytically by the techniques described in Appendix A of Ref. 14 and, for the sake of simplicity, we will not give the explicit formulas here.

To perform the $\mathbf{k}$ integration in Eqs. (10) and (11) we use the so-called special point sets,[23–25] apply the Hellmann–Feynman-like relation[26]

$$\nabla_{\mathbf{k}}E_{n\mathbf{k}}=\underline{A}^\dagger_{n\mathbf{k}}[\nabla_{\mathbf{k}}\underline{H}_{\mathbf{k}}-E_{n\mathbf{k}}\nabla_{\mathbf{k}}\underline{O}_{\mathbf{k}}]\underline{A}_{n\mathbf{k}} \tag{13}$$

[which is easily verified by differentiating (4) with respect to $\mathbf{k}$ (Refs. 14 and 27)] to obtain $\nabla_{\mathbf{k}}E_{n\mathbf{k}}$, and carry out a Gilat-Raubenheimer[28] integration. Compared with the tetrahedron method[29] this special Gilat-Raubenheimer procedure reduces, even when counting in the evaluation of (13), the computation time by a factor of 2 while it reaches the same accuracy.[30]

The total charge density n of the crystal is obtained by adding the charges $-eZ_\mu$ of the nuclei to the charge of the electrons (9) whereby the requirement of electrostatic neutrality of the whole system leads to the condition[31]

$$\Omega\rho^{(1)}_0=\sum_{\mu=1}^{M}\rho^{(2)}_\mu \tag{14}$$

with

$$\rho^{(2)}_\mu=Z_\mu-\sqrt{4\pi}s^3_\mu\int_0^1 t^2P_{0\mu}(t)dt\ . \tag{15}$$

Numerically, (14) is used as a test for the representation (12) and was fulfilled within 10^{-10} in every calculation showing that (12) provides a powerful tool in describing any oscillating behavior.

C. The effective potential

Within the Hohenberg-Kohn-Sham formalism[1] the effective potential is given by a sum of the electrostatic potential U and the exchange-correlation potential $V_{\mathrm{xc}}(r)=\delta E_{\mathrm{xc}}[\rho]/\delta\rho(\mathbf{r})$ with the exchange-correlation energy E_{xc} of the electron gas with density $\rho(\mathbf{r})$. The techniques we discuss here extend the considerations of Bross and Eder[3] beyond the warped muffin-tin approximation.

To construct the electrostatic potential we use requirement (14) to separate the total charge in Ω into four parts

$$\begin{aligned} n(\mathbf{r})/e=&\frac{1}{\Omega}\sum_{\mu=1}^{M}\rho^{(2)}_\mu[1-\Omega\delta(\mathbf{r}-\mathbf{R}_\mu)]\ \ [=n_1(\mathbf{r})]\\ &+\sum_{\mu=1}^{M}\sum_{0<L}t^l_\mu P_{L\mu}(t_\mu)Y_L(\hat{\mathbf{t}}_\mu)\ \ [=n_2(\mathbf{r})]\\ &+\sum_{\mu=1}^{M}\left[(\rho^{(2)}_\mu-Z_\mu)\delta(\mathbf{r}-\mathbf{R}_\mu)+\frac{P_{0\mu}(t_\mu)}{\sqrt{4\pi}}\right]\\ &\qquad\qquad[=n_3(\mathbf{r})]\\ &+\sum_{0<G_j\le G_{\max}}\rho^{(1)}_{\mathbf{G}_j}\exp(i\mathbf{G}_j\cdot\mathbf{r})\ \ [=n_4(\mathbf{r})]\ . \end{aligned} \tag{16}$$

This allows us to evaluate the Coulomb potential easily, because each term for itself has a vanishing mean value over Ω.

The contribution U_1 of n_1, the point charges with

strength $-\rho_\mu^{(2)}$ at site $\mathbf{R}_\mu$ counterbalanced by a uniform background charge, reads in Rydberg atomic units (i.e., $\hbar=1, m=\frac{1}{2}$, and $e^2=2$)

$$U_1(\mathbf{t}_\mu)=-2\sum_{\nu=1}^{M}\rho_\nu^{(2)}\left[\delta_{\mu,\nu}t_\nu^{-1}+\frac{2\pi}{3\Omega}t_\mu^2+\sum_L\frac{\beta_L^{\mu,\nu}}{a_{\mu,\nu}}\left[\frac{t_\mu}{a_{\mu,\nu}}\right]^l Y_L(\hat{\mathbf{t}}_\mu)\right] \quad (17)$$

and is designed from a special inhomogeneous solution in $\mathcal{H}_\mu$ (first two terms in the square brackets) and a general homogeneous part. The coefficients $\beta_L^{\mu,\nu}$ of the latter exclusively depend on the crystal structure and need to be evaluated only once for each type of lattice and the $a_{\mu,\nu}$ are scaling coefficients. Explicit expressions for $\beta_L^{\mu,\nu}$ and $a_{\mu,\nu}$ are found by the Ewald technique outlined in the Appendix.

In the same manner the potential produced by the multipoles n_2 can be written as

$$U_2(\mathbf{t}_\mu)=\sum_{L>0}\mathcal{S}_L^\mu(t_\mu)Y_L(\hat{\mathbf{t}}_\mu)+\sum_L\sum_{\nu=1}^{M}\gamma_L^{\mu,\nu}t_\mu^l Y_L(\hat{\mathbf{t}}_\mu) \quad (18)$$

with

$$\mathcal{S}_L^\mu(t)=\frac{8\pi s_\mu^2}{2l+1}\left[t^{1-l}\int_0^t u^{2l+2}P_{L\mu}(u)du+t^l\int_t^1 uP_{L\mu}(u)du\right]. \quad (19)$$

Contrary to (17) the expansion coefficients $\gamma_L^{\mu,\nu}$ of the homogeneous solution in (18) do not only depend on the crystal structure but also on all multipole strengths $\mathcal{S}_L^\nu(1)$. Their explicit evaluation involves also the $\beta_L^{\mu,\nu}$ and the Gaunt coefficients. This is also described in the Appendix.

Using (15) we find that the spherical charges n_3 contribute to the Coulomb potential by

$$U_3(t_\mu)=-2\frac{Z_\mu-\rho_\mu^{(2)}}{t_\mu}+\frac{\mathcal{S}_0^\mu(t_\mu)}{\sqrt{4\pi}} \quad (20)$$

in $\mathcal{H}_\mu$ only, and since the moment of n_3 vanishes over each sphere $\mathcal{H}_\mu$ it is zero everywhere outside $\mathcal{H}_\mu$.[3,31]

Finally, the potential U_4 due to the smooth plane-wave part n_4 is

$$U_{4L}(\mathbf{t}_\mu)=8\pi i^l\sum_{0<G_j<G_{\max}}\frac{\rho_{\mathbf{G}_j}^{(1)}}{G_j^2}j_l(G_j s_\mu t_\mu)\times Y_L(\hat{\mathbf{G}}_j)\exp(i\mathbf{G}_j\cdot\mathbf{R}_\mu) \quad (21)$$

and can be shown to be real by accounting for the symmetry of the $\rho_{\mathbf{G}_j}^{(1)}$. Owing to the linearity of Maxwell's equations the entire electrostatic potential U is given by the sum of U_1 up to and including U_4.

The exchange-correlation potential V_{xc} in $\mathcal{H}_\mu$ is given by the integral

$$V_{\mathrm{xc},L}(t_\mu)=\int_{\partial K(t_\mu,\mathbf{R}_\mu)}\frac{\delta E_{\mathrm{xc}}}{\delta\rho(t_\mu\hat{\mathbf{e}})}Y_L(\hat{\mathbf{e}})d^2e \quad (22)$$

extended over the surface of the sphere with radius t_μ centered at $\mathbf{R}_\mu$ which we evaluate numerically using 40 equidistant intervals for the φ direction and the Gauss formula with half of the number of points in the θ direction.

Besides the **r** representation in the spheres $\mathcal{H}_\mu$ the potential also enters the SAPW scheme by its Fourier coefficient. The corresponding expressions can be evaluated straightforwardly (using the **r** representation in the spheres and the Fourier representation in $\mathcal{I}$) but they are lengthy and, therefore, we omit them here.

D. The total energy

The Hohenberg-Kohn-Sham formalism[1] yields the total energy per unit cell as a sum of the band energies and the Coulomb energy of the protons at the atomic sites minus a term that corrects for double counting parts of the electron-electron interaction. Thereby, as was proven generally in **r** (Refs. 4 and 9) and in **p** space,[32] the infinite Coulomb energy of the protons and an infinite correction to the Coulomb energy of the electrons cancel each other exactly. Using this result we obtain in LDA with $E_{\mathrm{xc}}[\rho]=\int d^3r\,\rho\varepsilon_{\mathrm{xc}}(\rho)$,

$$E_{\mathrm{tot}}=\frac{2\Omega}{(2\pi)^3}\sum_n\int_{E_{n\mathbf{k}}\le E_F}d^3kE_{n\mathbf{k}}+\int_\Omega d^3r\rho\left[\varepsilon_{\mathrm{xc}}(\rho)-V_{\mathrm{eff}}+\frac{U}{2}\right]-\sum_{\nu=1}^{M}Z_\nu C_\nu, \quad (23)$$

where C_ν is, apart from a constant, the value of the Hartree potential at site ν which can be expressed by the coefficients $\beta_L^{\mu,\nu}$ and $\gamma_L^{\mu,\nu}$

$$C_\nu=\sum_{\mu=1}^{M}\left[\frac{\gamma_{l=0}^{\mu,\nu}}{2}-\rho_\mu^{(2)}\frac{\beta_{l=0}^{\mu,\nu}}{a_{\mu,\nu}}\right]+\sqrt{4\pi}\sum_{0<G_j\le G_{\max}}\frac{\rho_{\mathbf{G}_j}^{(1)}}{G_j^2}\exp(i\mathbf{G}_j\cdot\mathbf{r})+\sqrt{4\pi}s_\nu^2\int_0^1 tP_{l=0\mu}(t)dt \quad (24)$$

and $\varepsilon_{\mathrm{xc}}$ stands for the exchange and correlation energy density of an interacting homogeneous electron gas with density ρ. For further applications it might become important that (23) holds indeed for several nonlocal functionals E_{xc} involving derivatives of ρ.

III. NUMERICAL RESULTS

Since the pioneering work of Chodorow[33] the electronic structure of Cu has been investigated self-consistently by frequent theoretical work[18,34,35–38] and its narrow *s-d* valence-band complex provides a severe test of the accuracy for any calculation scheme. Because correlations are not too important in Cu, it turns out to be sufficient enough to use the exchange and correlation energy in the

parametrization of Hedin and Lundqvist[39] with numerical parameters of Gunnarson and Lundqvist.[40] What is more, this choice enables us to compare our results directly with the previous data of Moruzzi, Janak, and Williams and, thereby, to study the local-density limit.

In what follows we first discuss the convergence of the ground-state and structural properties of Cu. Therefore we use self-consistent effective potentials of general shape in the sense of (6) and in warped muffin-tin approximation (WMT). In this approximation we neglect the nonspherical terms in $\mathcal{K}_\mu$ and, in addition, the contributions of the electrostatic multipoles U_2 since they would bring in only a constant shift in each sphere.[3]

The accuracy of the SAPW band calculation itself is determined by the choice of the ansatz parameters: angular momentum limit $\lambda=2$, a number of B splines $N(l)=32$, $l=0,1,2$, and the plane-wave cutoff $q=(2\pi/a)\times 3.89$ with the cubic side lattice constant a. For the occupied bands in Cu this choice leads to an *ad hoc* error that is less than 0.10 mRy for the one-particle energies as we found by intrinsic convergence tests and by comparing our band energies to the results of a highly converged MAPW calculation.

We used 10 special points for **k** integration during their first self-consistent iterations, while final convergence and the results were obtained with a 60 special points mesh.

A. Influence of the shape of the effective potential

We start to investigate the convergence of the shape approximations by considering the band energies and the wave functions.

Table I shows the energies for one **k** point out of the ten special points integration mesh in WMT and for two nonspherical potentials characterized by the angular momentum cutoff $l_p=8$ (FP8) and $l_p=14$ (FP14). In order to obtain the exchange-correlation potential, we used a larger cutoff l_p+4 for the charges $P_{L\mu}$. First of all, we observe that FP8 gives a sufficient description of the band energies within 0.1 mRy and note that the sum of the energies over all occupied bands in the total energy (23) will converge, even in WMT, more rapidly since, for different bands, the corrections WMT-FP8 show the tendency to cancel each other. Secondly, the energies of the high core states (and of the not shown $1s$, $2s$, and $2p$ states) are more negative for a potential of general shape. As it turns out, the self-consistent calculation redistributes the electron charges and localizes the valence electrons more near the nuclei. Thirdly, the valence-band energies show moderate modifications up to roughly 2 mRy in magnitude and alternating sign. Thereby, the interband distances in the narrow s-d band complex are altered by up to 10%.

TABLE I. Band energies relative to the Fermi energy in mRy at the special point $\mathbf{k}=\pi/4a(3,1,1)$ and lattice constant 6.6945 a.u. near the calculated equilibrium value for the high-core levels ($3s$ and $3p$), the valence bands, and the first conducting band. The completely hybridized bands 10–15 are labeled by their band numbers. WMT stands for the warped muffin-tin approximation and FP8 and FP14 denote truncation values of $l_p=8$ and $l_p=14$ in the multipole expansion of the potential (6), respectively.

Band	WMT	FP8	FP14
6($3s$)	−7943.3	−7943.5	−7943.5
7($3p$)	−5048.7	−5048.9	−5048.9
8($3p$)	−5043.7	−5043.8	−5043.8
9($3p$)	−5042.9	−5043.0	−5043.0
10	−379.4	−377.3	−377.3
11	−344.0	−345.5	−345.6
12	−170.0	−170.9	−170.9
13	−152.0	−151.5	−151.5
14	−126.3	−126.6	−126.5
15	107.6	106.0	106.0

However, the more interesting point is the behavior of the wave function. Since the variational principle of quantum mechanics guarantees that, in relation to a change in the wave function, the energy is less affected, moderate changes of the energies might be connected to significant modifications of the wave functions. The most important effect in the case of a nonspherical potential is the split-up of the radial functions R_l into R_{lm} which arises from the coupling of the radial Schrödinger equations. We govern this effect by comparing our results ($R_L=R^{(1)}_{L\mu}+R^{(2)}_{L\mu}$) at a **k** point without symmetry to the result an energy derivative technique would yield

$$R^{\rm ed}_L(r;E)=a_{lm}f_l(r;E)+b_{lm}\dot{f}_l(r;E)\ , \tag{25}$$

where f_l denotes the solution of the radial Schrödinger equation with the spherical part of the potential and the dot denotes the energy derivative.[6,7] These functions are used, e.g., in all FLAPW and LMTO (linearized-muffin-tin-orbital[7]) schemes. Thus, because there are two coefficients in (25), at most two linear independent functions can be found among the entity of the $R^{\rm ed}_L$ while there are, in general, $2l+1$ for a **k** point without symmetry. For this reason, one expects the neglect of the coupling to be large at higher values of l. To be specific, there are three linear independent p functions but five d functions while the energy derivative technique supports only two of them in both cases. The coefficients a_{lm} and b_{lm} in (25) are fixed to match the plane-wave part in $\mathcal{J}$ with a continuous first derivative and we used our result in $\mathcal{J}$ for this fit. In general, the difference $R_L-R^{\rm ed}_L$ depicts the errors which arise from neglecting the coupling of the radial equations as well as from the linearization by the energy derivative technique. In order to isolate the first effect, we consider a single band and minimize the linearization error by setting $E\approx E_{n\mathbf{k}}$ in (25). To ensure the convergence of the fit we used a larger value $q=(2\pi/a)\times 4.37$ for the plane-wave cutoff than in all other calculations. If $E=E_{n\mathbf{k}}$ exactly, in the limit $q\to\infty$, and in case of a muffin-tin potential, it follows from the original formulation of the augmented plane waves by Slater[41] that $b_{lm}=0$.

Figure 1 displays the differences between the R_L and the $R^{\rm ed}_L$ for $l=2$, two different values of m, and the highest valence band. The energy E was chosen roughly to minimize the differences $R_L-R^{\rm ed}_L$, so that this $R^{\rm ed}_L$ is the best estimate which can be obtained by the energy derivative technique. For a best estimate the deviations

are remarkably large in both cases even though smaller differences occur for the three other values of m which are not shown. As it is expected in a general $\mathbf{k}$ point, there exists five linearly independent R_L for $l=2$ while there are only two R_L^{ed}. We find that the R_L evaluated by the variational procedure including nonspherical parts of the potential are more localized than the R_L^{ed}. A similar behavior is found also for other $\mathbf{k}$ points, and is responsible for the more tightly bound behavior of the valence electrons in our FP8 calculation. The magnitude of the differences in Fig. 1 proves the necessity to use R_{lm} (instead of R_l) to adequately treat a nonspherical potential.

Figure 1 does not only exemplify the magnitude of the split-up of the R_l into R_{lm} but also gives an idea of the magnitude of the error of the full-potential treatment in FLAPW. However, this error, on the one hand, is overestimated by the deviations depicted in Fig. 1 since its estimation entails two further aspects: First of all, just matching R_L^{ed} on our solution in $\mathcal{J}$ violates the normalization of $\Psi_{n\mathbf{k}}$. Secondly, for the same reason, the R_L^{ed} are no longer a variational solution of the Schrödinger equation. The correction of both defects will, due to the variational principle, diminish the error. Nevertheless the outcome of the differences is larger than one would expect from the magnitude of other full-potential effects.

On the other hand, by considering the best estimate with respect to the energy E, we tried to neglect the linearization error in our investigations which depends on the energy difference $E-E_{n\mathbf{k}}$ and can become almost a magnitude larger than the split-up effect shown in Fig. 1. In addition, this linearization error sensitively depends on the number of plane waves that enters the calculation by the logarithmic derivative at the sphere boundary. When we increased the plane-wave cutoff from $(2\pi/a)\times 3.89$ (i.e., 60 plane waves) to $(2\pi/a)\times 4.37$ (i.e., 84 plane waves) our R_L were not visibly modified while in case of the R_L^{ed} the larger value of q was necessary to achieve convergence.

In conclusion, even the best estimate of the usual energy derivative technique cannot describe the correct split-up in the case of d states and needs a larger plane-wave cutoff to ensure convergence when compared with our results.

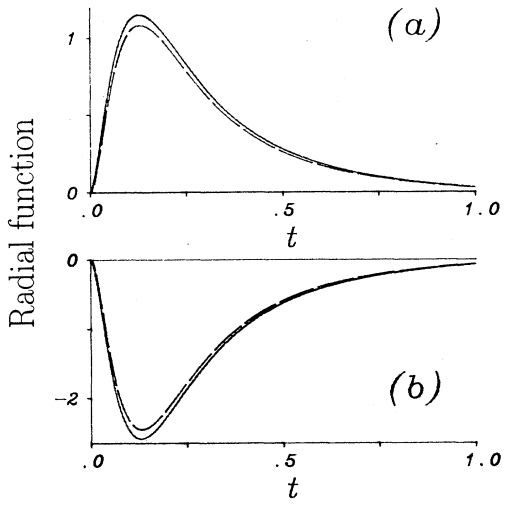

FIG. 1. Radial functions at point $\mathbf{k}=\pi/4a(1,2,3)$ for the highest valence band, $l=2$, and two different types of d functions: (a) $\propto P_l^0(z)$; (b) $\propto P_l^2(z)\sin(2\varphi)$ in arbitrary units. The solid lines are the SAPW results of a FP8 calculation as explained in Table I and the broken lines depict the results of the energy derivative technique R_L^{ed} for the energy $E=200$ mRy. The energy of the band is 204.7 mRy. This is the best agreement that can be obtained by minimizing the linearization error of the energy derivative technique and accounting for its slower convergence with respect to the number of plane waves. For the three other types of d functions these best results of the energy derivative technique almost coincide with the SAPW functions.

B. Ground-state and related properties of Cu

The charge density is the fundamental quantity of the density-functional formalism and can, on the other hand, be measured directly by the form factors of x-ray scattering or by γ-ray diffractometry. Having in mind the shape restrictions of the potential, the crystal anisotropy which occurs first at the (511) vs (333) reflection is of particular interest.

In Table II we list experimental data of Jennings, Chipman, and DeMarco,[42] Freund,[43] Schneider, Hansen, and Kretschmer,[44] and Temkin, Henrich, and Raccah[45] together with our results FP8 and WMT and the values of previous theoretical work of MacDonald *et al.*[35] Unfortunately, because of the large atomic number of Cu the experiments are difficult and the available data scatter considerably (sometimes even with nonoverlapping error bars) and furthermore, only Schneider, Hansen, and Kretschmer are able to access any experimental difference between the (511) and the (333) reflection and this value lies within their error bars.

Comparing first our results for the shape approximations WMT and FP8 we observe negligible differences except for those reflections where the anisotropy plays an important role. In Table II this is demonstrated for the reflections (511) and (333): While the FP8 results show a significant difference between the (511) and the (333) reflections no anisotropy effect occurs (within the listed digits) in the WMT calculation. Contrary to the charge redistributions between core and valence states individually which we found in the last section, the total charge is scarcely influenced by restrictions on the shape of the potential. Only the anisotropy reacts sensitively.

Our theoretical results lie always in the uncertainty region between the different experimental data and are in good overall agreement with the mean values of the x-ray measurements of Temkin *et al.*: The differences are always smaller than 0.3%, except for the (111) and (400) reflection where they are about 1%. Therefore, we suspect that these data are more accurate than their large error bars suggest.

Moreover, we found that the form factors $f_{(hkl)}(a)$, as functions of the lattice constant, behave like

$$f_{(hkl)}(a)=f_{(hkl)}(\bar{a})+(a-\bar{a})g_{(hkl)} \tag{26}$$

TABLE II. Experimental and theoretical values of the form factors. Our calculations WMT and FP8 were carried out with the lattice constant $a=6.8312$ a.u. near room temperature. The x-ray experiments of Jennings, Chipman, and DeMarco, Freund, and Temkin, Henrich, and Raccah were also performed at room temperature, while Schneider, Hansen, and Schneider worked at 50 K which corresponds to $a=6.809\,63$ a.u. The errors of the experimental data are given in parentheses. Other notations are explained in Table I.

(*hkl*)	Jennings, Chipman, and DeMarco[a]	Freund[b]	Schneider, Hansen, and Kretschmer[c]	Temkin, Henrich, and Raccah[d]	This work WMT	This work FP8	MacDonald *et al.*[e]
(111)	21.52(10)	22.63	21.38(9)	21.93(15)	21.729	21.731	21.73
(200)			20.10(6)	20.36(15)	20.405	20.400	20.39
(220)			16.45(5)	16.70(16)	16.675	16.674	
(311)			16.54(4)	14.71(17)	14.747	14.747	
(222)	14.01(10)	14.64(10)	13.99(8)	14.18(17)	14.212	14.212	14.25
(400)			12.29(6)	12.33(20)	12.464	12.464	
(333)	9.41(10)	9.45(10)	9.45(9)		9.618	9.612	9.66
(511)			9.49(6)		9.618	9.626	9.67

[a]Reference 42.
[b]Reference 43.
[c]Reference 44.
[d]Reference 45.
[e]Reference 35.

in a large region around the equilibrium $\bar{a}$. The expansion coefficients $g_{(hkl)}$ are listed in Table III and vary only slightly with the index of the reflection. With these parameters it is possible to reduce the differences to the complete γ-ray data set of Schneider, Hensen, and Kretschmer significantly taking into account that their experiments were performed at 50 K, corresponding to a lattice parameter $a=6.80963$ a.u., while our calculations were performed with a lattice parameter near room temperature, where the other experiments were carried out. With the correction (26) the discrepancies between our results and Schneider's experiment become generally smaller than 1.5%.

The differences between our data and the theoretical values of MacDonald *et al.* are small, strikingly when compared with the deviations from the experimental results and with the fluctuations among them. This is quite remarkable because MacDonald *et al.* used a different calculation scheme and a different approximation for the exchange and correlation energy. The first fact shows again that the total charge density reacts insensitively on computational details while the latter supports our former assumption that the exact form of the correlation functional plays no important role in the case of Cu when dealing with the charge density.

Beside the charge density the total energy of the electronic system, as a function of the volume or the lattice constant, is a ground-state property and can be used to calculate structural properties. Our calculated total energies for lattice parameters in a range of 10% around the experimental value excellently fit in the interpolation formula

$$E_{\text{tot}}(\Omega)=C_1+C_2/\Omega+C_3/\Omega^2 \tag{27}$$

near the equilibrium lattice constant $\bar{a}$ as well as in the universal expression of Rose, Ferrante, and Smith[46]

$$E_{\text{tot}}(a)=E^0_{\text{tot}}(1+x)\exp(-x) \tag{28}$$

with $x=C_4(a-\bar{a})$. The parameters of both formulas were calculated by least-mean-square fits and are listed in Table IV. From (27) we calculated the bulk modulus $B=-\Omega\partial P/\partial\Omega$. In Table V our results for $\bar{a}$, B, and the total energy at equilibrium E^0_{tot} (WMT and FP8) are compared with experimental data of Weast,[47] Overton and Gaffney,[48] as well as with the previous theoretical Korringa-Kohn-Rostoker (KKR) calculation of Moruzzi, Janak, and Williams.[18] For completeness, we also listed the result of an early configuration averaged *atomic* Hartree Fock (HF) calculation by Mann.[49] To obtain the experimental lattice constant at $T=0$, we used the results for the thermal expansion of Cu at low temperatures of Himmler *et al.*[50] Additionally, we included the effect of the zero-point energy within the Debye approximation

$$E_{\text{zp}}=9/8k_B\Theta_d(\Omega_0/\Omega)^g\,, \tag{29}$$

in our FP8 calculation, where $\Theta_d=336$ K (Ref. 51) is the Debye temperature, $\Omega_0=78.92$ is the corresponding atomic volume, $g=2.00$ (Ref. 51) is the Grüneisen constant, and k_B is the Boltzmann constant.

We find the total energy influenced only very little by

TABLE III. Linear expansion coefficients of the form factors as defined in Eq. (26) for the form factors in Table II.

(*hkl*)	$g_{(hkl)}$	(*hkl*)	$g_{(hkl)}$
(111)	1.340	(200)	1.490
(220)	1.769	(311)	1.811
(222)	1.808	(400)	1.734
(511)	1.386	(333)	1.390

TABLE IV. Parameters for the first of the calculated total energies in the energy curves of formulas (27) and (28) in a.u. Other abbreviations are explained in Table I.

	E^0_{tot}	$\bar{a}$	C_1	C_2	C_3	C_4
WMT	−3277.0518	6.6429	−3276.5726	−70.280 542	+2575.2936	$6.795\,440\,3\times10^{-3}$
FP8	−3277.5029	6.6398	−3276.5738	−70.177 540	+2567.8840	$6.780\,528\,6\times10^{-3}$

the shape of the potential, especially in comparison to the large deviations which occurred for the one particle energies and for the wave functions. The differences between our calculations for potentials of different shapes are less than 0.1% for the lattice constant and for the bulk modulus while the FP8 result for the equilibrium total energy lies 1.1 mRy below the WMT value. Contrary to that, the deviations between our results and the calculations of Moruzzi, Janak, and Williams are notably large: First of all, in the calculation of Moruzzi, Janak, and Williams the lattice constant as well as the bulk modulus agree much better with the experiment. Secondly, the value for the equilibrium total energy E^0_{tot} of Moruzzi, Janak and Williams lies 1.284 Ry above the value of our WMT calculation, although both calculations are based upon the same approximation for the exchange and correlation energy. From the variational principle[1] the lower value is always the more accurate one. Moreover, because our calculations show that the influence of shape approximations is in the magnitude of mRy's, we conclude that the muffin-tin approximation in the calculations of Moruzzi, Janak, and Williams cannot be solely responsible for the large deviations. This might indicate that Moruzzi, Janak and Williams possibly made too rough truncations within their Greens-function scheme or within other numerical approximations that were necessary to enable their calculation. Another hint can be taken from the configuration averaged atomic HF result of Mann, which lies again 0.8 Ry below our equilibrium value. Although this old calculation should not be expected to be very precise from the viewpoint of today, a HF calculation neglects correlation but treats the exchange energy exactly by definition. Therefore, it is partially more accurate than any LDA calculation. Since the correlation energy is always negative, and the solid is more stable than the free atom, the atomic HF value marks an upper limit for any solid calculation, also. Nevertheless, our values for E^0_{tot} remain above Mann's result but we ascribe this failure to the LDA in principle. From our investigations the value of −3277.053 Ry represents the local-density limit in the case of Cu, at least for the correlation-energy functional of Gunnarson and Lundqvist and when neglecting relativistic effects. This demonstrates a need for a nonlocal treatment of exchange and correlation for a further significant improvement.

TABLE V. Calculated lattice constant $\bar{a}$ (a.u.), bulk modulus B (mbar), and total energy E^0_{tot} (Ry) at equilibrium. The abbreviations WMT and FP8 are explained in Table I while FP8+ZP denotes that the zero-point energy is included within the Debye approximation in the FP8 calculation. For comparison, we listed the experimental values for different temperatures, the results of a self-consistent Greens-function (KKR) calculation, and the absolute value of the total energy of a configuration averaged *atomic* Hartree-Fock (HF atom) calculation.

	$\bar{a}$	B	E^0_{tot}
WMT	6.6429	1.925	−3277.0518
FP8	6.6398	1.927	−3277.0529
FP8+ZP	6.6529	1.902	−3277.0493
Expt. (T=298 K)	6.8314(9)[a]	1.371[b]	
Expt. (T=0 K)	6.8107(9)[c]	1.420[b]	
KKR	6.76[d]	1.55[d]	−3275.768[d]
HF atom			−3277.928[e]

[a]Reference 47.
[b]Reference 48.
[c]References 47 and 50.
[d]Reference 20.
[e]Reference 49.

As usual in LDA, our calculation underestimates the equilibrium lattice constant while it overestimates the bulk modulus when compared to experiment. If we neglect the zero-point energy the lattice constant comes out 2.5% too small while the bulk modulus is 36% too large. Including the zero-point correction (29), the deviation of $\bar{a}$ is reduced to 2.3% while the error for the bulk modulus is still 33%. These errors are characteristical for the LDA in sign and magnitude. Thus, taking together all observations we conclude that the less accurate calculation of Moruzzi, Janak, and Williams caused values of $\bar{a}$ and B that are in better agreement with the experiment than the LDA can predict, in particular, with the form of exchange and correlation employed.

Contrary to the form factors and to the total energy, the LDA one-particle energies are no ground-state property and have no direct physical meaning. Most importantly, they must not be interpreted as quasiparticle energies. Therefore it is precarious to compare them with, e.g., photoemission data. Nevertheless, from a pragmatic point of view, the LDA eigenvalues should reveal a reasonable approximation to the quasiparticle energies in the case of metals and if states close to the Fermi level are considered. Figure 2 displays the valence bands of our FP8 calculation along the Σ and S directions in the first Brillouin zone together with the results of a previous self-consistent LCGO investigation of Bagayoko *et al.*[36] and the results of angle-resolved photoemission.[52] While our calculation was carried out near the experimental value of the lattice constant at room temperature, no value was reported for the LCGO calculation which also employs a different local exchange and correlation potential proposed by Rajagopal.[53]

Figure 2 demonstrates that the LDA eigenvalues describe the energy bands quite satisfactorily along both directions and as it is expected the deviation from the

photoemission data enlarges if bands move away from the Fermi level. Near E_F only the $\Sigma_1^{(3)}$ level deviates remarkably from the experimental values. However, our result shows a better overall agreement with the experimental data than the LCGO bands along the Σ direction, mainly the $\Sigma_1^{(1)}$ band and the Σ_3 and Σ_4 bands near point K are improved. A different behavior is observed along the S direction where the lack of consistency between experimental data and theoretical results is larger in general. It remains uncertain if the lower cascade of photoemission peaks along the S direction stems from the first or the second S_1 band. Also the higher sample of experimental values along this direction can only be approximately interpreted to describe the S_4 band. The differences between the calculated and the observed bands can be ascribed to the Hohenberg-Kohn-Sham formalism in general. Therefore, from Fig. 2 one would expect self-energy corrections for the LDA results to be large for Σ_1 bands (which are delocalized s-like states) and along direction S but small in the other cases. The differences between the two theoretical calculations are originated in a possibly different lattice constant (which seems to be smaller in the LCGO calculation), in differences in the calculation schemes for the band structure and for the self-consistent potential, and in other exchange and correlation potentials, but cannot be reliably assigned to one of these reasons in particular.

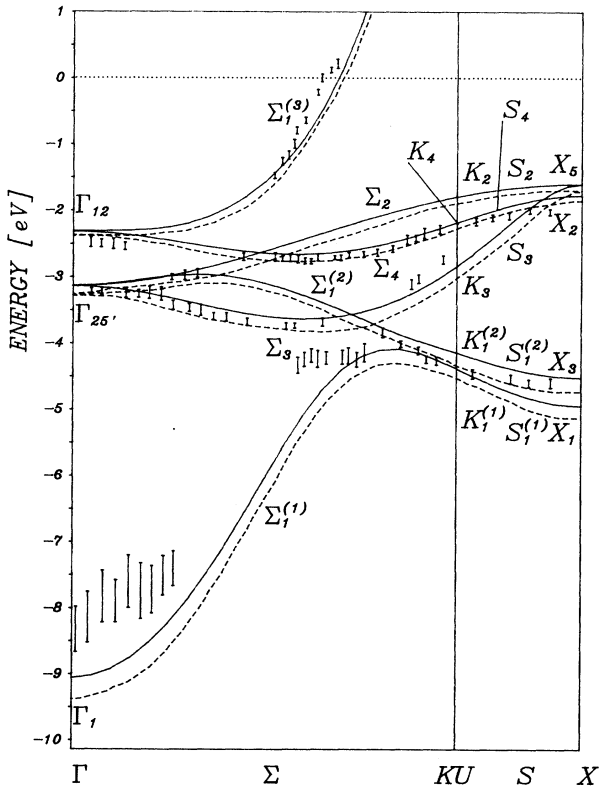

FIG. 2. Band energies and photoemission data along the directions Σ and S. The solid line depicts our FP8 results with lattice parameter $a=6.8312$ a.u. while the dashed line shows the result of a self-consistent LCGO calculation of Bagayoko, Laurent, and Singhal (Ref. 36). The experimental data were taken from Thirty *et al.* (Ref. 52).

IV. CONCLUSIONS

The SAPW method is a linear, self-consistent, all-electron, full-potential scheme which combines the attributes of exact orthogonality of all states to each other, a well-defined error of the final Ritz procedure, and completeness of the basis set.

For Cu, full-potential effects are in the order of 2 mRy for the energy bands and 1 mRy for the total energy. The ground-state properties are not much affected by the shape of the potential, except those form factors which reveal the crystal anisotropy. The most surprising fact is that the valence electrons behave perceptibly more tightly bond and that the split-up of the R_l into R_{lm} is responsible for this behavior. Our absolute value of the total energy at equilibrium is lower than the value of the former calculation of Moruzzi, Janak, and Williams[18] and indicates that nonlocal effects become important for further essential progress.

For Cu some attempts exist to include nonlocal effects of exchange and correlation in the framework of the density-functional theory: Norman and Koelling[37] used the Langreth-Mehl gradient correction[54] to the LDA and Przybylski and Borstel[38] constructed nonlocal exchange and correlation potentials from the pair-distribution function of the homogeneous electron liquid. Unfortunately, these authors focused their interest on the band energies and on the Fermi surface but did not calculate the total energy or other ground-state properties. Thus no clues about the magnitude of nonlocal effects on the ground-state and structural properties of Cu exist.

However, the recent development of the generalized-gradient approximation (Ref. 55) seems to be more promising than previous approaches: Current calculations for the alkali metals show that the GGA predict the structural properties in better agreement with the experiment than the LDA does.[55] In addition, calculations of the total energies of spherically symmetric atoms (with exchange only) reach almost the Hartree-Fock results.[56] This suggests that the GGA, in particular, for the exchange energy, might be a useful approach beyond LDA for Cu.

The tools to improve the band energies are different, since the deviation of the band energies from measured photoemission peaks is not a failure of the LDA but of the Hohenberg-Kohn-Sham formalism in general. Therefore, an advanced scheme has to involve the self-energy operator, e.g., in GW approximation[57] which includes a screened and nonlocal interaction as well as lifetime broadening. The SAPW method is well suited for this purpose because its complete basis set enables a reliable evaluation of the dielectric response, also.

APPENDIX: PROTON AND MULTIPOLE CONTRIBUTIONS TO THE POTENTIAL OF A CRYSTAL

As is generally recognized, the Coulomb potential of any periodic system can be determined approximately by

the pseudocharge method.[11,58] In contrast to that we use an improved Ewald[31,59] technique following the ideas of one of us,[60] which gives the exact result. Additionally, we gain an insight into the convergence properties of the multipole expansion (6) of the crystal potential.

1. The contribution of the protons

The charge density $n_1^\mu(\mathbf{r})$ in the first cell, which in accord with (16) is defined by $n_1(\mathbf{r})=\Omega^{-1}\Sigma_{\mu=1}^{M} n_1^\mu(\mathbf{r})$, possesses the Fourier transform

$$n_1^\mu(\mathbf{G})=\begin{cases}-\rho_\mu^{(2)}\exp(-i\mathbf{G}\cdot\mathbf{R}_\mu) & \mathbf{G}\neq\mathbf{0}\\ 0 & \mathbf{G}=\mathbf{0}.\end{cases} \tag{A1}$$

As a result, besides an arbitrary constant, the Coulomb potential is given by the series

$$U_1^\mu(\mathbf{r})=-8\pi\rho_\mu^{(2)}\sum_{\mathbf{G}\neq 0}\exp[i\mathbf{G}\cdot(\mathbf{r}-\mathbf{R}_\mu)]/G^2\ , \tag{A2}$$

which is at best conditionally covergent, so that we must not interchange the sum and the integral when substituting $\int_0^\infty \exp(-G^2t)dt$ for G^{-2}. By careful but straightforward manipulation one obtains

$$U_1^\mu(\mathbf{r})=-8\pi\rho_\mu^{(2)}\left[\frac{\Omega}{8\pi^{3/2}}\sum_{\mathbf{R}^n}\int_0^{\eta^2}\exp[(\mathbf{r}-\mathbf{R}_\mu^n)^2/4t]t^{-3/2}dt-\eta^2+\sum_{\mathbf{G}\neq 0}\frac{\exp[i\mathbf{G}\cdot(\mathbf{r}-\mathbf{R}_\mu)-G^2\eta^2]}{G^2}\right], \tag{A3}$$

where $\mathbf{R}_\mu^n$ denotes the vector to site μ in cell n and the split-up parameter η ensures the absolute convergence of both sums over $\mathbf{R}^n$ and $\mathbf{G}$, individually. Therefore we are able to expand each term around site $\mathbf{R}_\nu$

$$U_1^\mu(\mathbf{r})=\sum_L U_{1L}^{\mu,\nu}(t_\nu)Y_L(\hat{\mathbf{t}}_\nu)\quad \text{if } \mathbf{r}\in\mathcal{K}_\nu\ , \tag{A4}$$

and obtain from (A3)

$$U_{1L}^{\mu,\nu}(t_\nu)=-8\pi\rho_\mu^{(2)}\left[-\delta_{l0}\sqrt{4\pi}\eta^2+\frac{\Omega}{\sqrt{4\pi}}\sum_{\mathbf{R}^n}Y_L(\hat{\mathbf{R}}_{\mu-\nu}^n)\int_0^{\eta^2}j_l\left[\frac{\tau_\nu R_{\mu-\nu}^n}{2ti}\right]\exp\left[-\frac{\tau_\nu^2+(R_{\mu-\nu}^n)^2}{4t}\right]t^{-3/2}dt\right.$$
$$\left.+4\pi\sum_{\mathbf{G}\neq 0}\exp(-G^2\eta^2-i\mathbf{G}\cdot\mathbf{R}_{\mu-\nu})j_l(\tau_\nu G)/G^2Y_L(\hat{\mathbf{G}})\right] \tag{A5}$$

therein we used the generating function of the spherical Bessel functions j_l, $\mathbf{R}_{\mu-\nu}^n=\mathbf{R}_\mu^n-\mathbf{R}_\nu$, and $\tau_\nu=\mathbf{r}-\mathbf{R}_\mu$. Complementary to (A5), we know from electrostatics[61] that the solution of Poission's equation can be, at least in the immediate vicinity of site $\mathbf{R}_\mu$, set down in the form (17). For $l>0$ we expand (A5) into powers of τ_ν and compare each power with the corresponding term in (17) to obtain the coefficients $\beta_L^{\mu,\nu}$. Integrating l times by parts, we are left with

$$\beta_L^{\mu,\nu}=4\pi a_{\mu\nu}^{l+1}\left\{\frac{1}{2l+1}\sum_{\mathbf{R}^n}'\left[\frac{1}{\sqrt{\pi}\eta}\sum_{m=0}^{l-1}\frac{(R_{\mu-\nu}^n/\eta)^{2m}}{2^m(2m+1)!!}\exp\left[-\frac{(R_{\mu-\nu}^n)^2}{4\eta^2}\right]-\frac{\operatorname{erfc}(R_{\mu-\nu}^n/2\eta)}{R_{\mu-\nu}^n}\right]\frac{Y_L(\hat{\mathbf{R}}_{\mu-\nu}^n)}{(R_{\mu-\nu}^n)^l}\right.$$
$$\left.+\frac{4\pi}{\Omega}\frac{1}{(2l+1)!!}\sum_{\mathbf{G}}'\frac{\exp(-G^2\eta^2)}{G^{2-l}}\mathcal{P}_{\mu\nu}^l(\mathbf{G})Y_L(\hat{\mathbf{G}}_j)\right\}, \tag{A6}$$

where erfc denotes the complementary error function, $a_{\mu\nu}$ is a scaling constant (see below) that ensures the independency of the $\beta_L^{\mu,\nu}$ from the volume Ω, and the prime on the sum indicates its extension over all values $\mathbf{R}^n$ and $\mathbf{G}$, respectively, for which the denominators do not vanish. The structure factor $\mathcal{P}_{\mu\nu}^l$ is given by

$$\mathcal{P}_{\mu\nu}^l(\mathbf{G})=\cos(\mathbf{G}\cdot\mathbf{R}_{\mu-\nu}-l\pi/2)\ . \tag{A7}$$

Since (A5) also includes the inhomogeneous solution, which is irregular at site $\mathbf{R}_\mu$, the case $l=0$ shows different behavior. However, we can expand U_{10}^μ into a Laurent series around $\mathbf{R}_\mu$ up to terms τ_ν^2, cancel the inhomogeneous contributions, and then compare with (17). We get

$$\beta_0^{\mu,\nu}=a_{\mu\nu}\sqrt{4\pi}\left[\sum_{\mathbf{R}^n}'\frac{\operatorname{erfc}(\mathbf{R}_{\mu-\nu}^n/2\eta)}{R_{\mu-\nu}^n}-\frac{4\pi}{\Omega}\left[\eta^2-\sum_{\mathbf{G}}'\frac{\exp(-G^2\eta^2)}{G^2}\mathcal{P}_{\mu\nu}^0(\mathbf{G})\right]-\frac{\delta_{\mu\nu}}{\sqrt{\pi}\eta}\right], \tag{A8}$$

which by (A2) guarantees the U^{μ}_{10} has vanishing mean value over Ω.

In (A6) and (A8) we have to choose the values of the split-up parameter η and the scaling coefficients $a_{\mu\nu}$: η controls the convergence of the sums over $\mathbf{R}^n_{\mu-\nu}$ and $\mathbf{G}$ in (A6) and (A8) and we found $\eta \approx 7.9\times\Omega^{1/3}$ to be quite a good choice. The results, of course, are independent of η. To find a meaningful value for the scaling coefficients $a_{\mu\nu}$ we chose it as the radius of convergence of the multipole expansion (A4) which can be found as follows: In the limit $\eta\rightarrow\infty$ (A6) becomes

$$\beta^{\mu,\nu}_L=\frac{4\pi a^{l+1}_{\mu\nu}}{2l+1}\sum_{\mathbf{R}^n}{}' \frac{Y_L(\hat{\mathbf{R}}^n_{\mu-\nu})}{(R^n_{\mu-\nu})^{l+1}} \quad \text{for } l>0 \tag{A9}$$

and can be found also by direct expansion of the Coulomb kernel[62]

$$\frac{1}{|\tau_\nu-\tau'_\mu-\mathbf{R}^n_{\mu-\nu}|}=\sum_L \frac{4\pi}{2l+1}\frac{\tau^l_<}{\tau^{l+1}_>}Y_L(\hat{\tau}_>)Y_L(\hat{\tau}_<) \tag{A10}$$

with $\tau'_\mu=\mathbf{r}'-\mathbf{R}_\mu$ and $\tau_{<(>)}=\min(\max)\{\tau_\nu;\tau'_\mu+\mathbf{R}^n_{\mu-\nu}\}$. The application of this expansion necessitates the conditions

$$|\tau_\nu|\le|\tau'_\mu-\mathbf{R}_{\mu-\nu}| \quad \text{if } \mu\neq\nu,\ \mathbf{R}^n=0 \text{ and } \mathbf{r}'\in\Omega \tag{A11}$$

for all distinct pairs ν and μ and

$$|\tau_\mu|\le|\tau'_\mu-\mathbf{R}^n| \quad \text{if } \nu=\mu,\ \mathbf{R}^n\neq 0 \text{ and } r'\in\Omega \tag{A12}$$

for all atomic sites μ to hold simultaneously, while the radius of convergence for each $U^{\mu,\nu}_{1L}$ separately is given by $\frac{1}{2}|\mathbf{R}_{\mu-\nu}|$ for $\mu\neq\nu$. Thus (A11) and (A12) can be fulfilled coincidently only by the choices

$$s_\mu\le\tfrac{1}{2}\min_{\mathbf{R}_\nu\neq\mathbf{R}_\mu}|\mathbf{R}_{\mu-\nu}| \text{ and } a_{\mu\nu}=\tfrac{1}{2}|\mathbf{R}_{\mu-\nu}|=a_{\nu\mu}\ , \tag{A13}$$

while at and beyond these radii the expansion (17) for the proton potential is invalid, in general. However, the conditions (A13) reveal no substantial restrictions because the corresponding choices of the spheres $\mathcal{K}_\mu$ is geometrically obvious. Moreover, it is possible to obtain a multipole representation for the proton potential even for $\tau_\nu>a_{\mu,\nu}$, if the nearest-neighbor terms in (A10) are treated differently and thereby the terms $\propto\tau_\nu^{1-l}$, which also are regular for $\tau_\nu>a_{\mu\nu}$, are taken into account. In the case of $\mu=\nu$ or one atom in the basis (A13) reduces to

$$s_\mu\le r_0 \text{ and } a_{\mu\mu}=r_0 \tag{A14}$$

where r_0 is half of the nearest-neighbor distance.

2. The contribution of the multipoles

The potential due to the multipoles n_2 in (16) reduces to the integral

$$U_2(\mathbf{t}_\nu)=2s^3_\mu\sum_{\mathbf{R}^n}\sum_{\mu=1}^{M}\sum_{L>0}\int_{K(0,1)}\frac{t^l P_{l\mu}(t)Y_L(\hat{\mathbf{t}})}{|\tau_\nu-s_\mu\mathbf{t}-\mathbf{R}^n_{\mu-\nu}|}d^3t \tag{A15}$$

extended over the unit sphere because $P_{l\mu}(t)=P'_{l\mu}(t)=0$ for $t\ge 1$, and can be rewritten as

$$U_2(\mathbf{t}_\nu)=\sum_{L>0}\mathcal{S}^\nu_L(t_\nu)Y_L(\hat{\mathbf{t}}_\nu)+\sum_{\mu=1}^{M}\sum_{L>0}\mathcal{S}^\mu_L(1)s^{l+1}_\mu\sum_{\mathbf{R}^n}{}'\frac{Y(\hat{\mathbf{T}}^n_{\mu-\nu})}{|\mathbf{T}^n_{\mu-\nu}|^{l+1}} \tag{A16}$$

with $\mathbf{T}^n_{\mu-\nu}=\tau_\nu-\mathbf{R}^n_{\mu-\nu}$. The sum in the last term has to be extended over all $\mathbf{R}^n$ for which $\mathbf{R}^n_{\mu-\nu}\neq 0$ and therefore is homogeneous in the neighborhood of $\tau_\nu=0$. Actually, studying the relation[63]

$$h^+_l(p|\mathbf{a}-\mathbf{b}|)Y_L(\mathbf{a}\hat{-}\mathbf{b})4\pi\sum_{L'L''}i^{l'-l''-l}C^L_{L',L''}j_{l'}(pa)h^+_{l''}(pb)Y_{L'}(\hat{\mathbf{a}})Y_{L''}(\hat{\mathbf{b}}) \quad \text{if } |\mathbf{a}|<|\mathbf{b}|\ , \tag{A17}$$

where h^+_l denotes the spherical Hankel function of first kind[62] in the limit $p\rightarrow 0$ we find

$$\frac{Y_L(\mathbf{a}\hat{-}\mathbf{b})}{|\mathbf{a}-\mathbf{b}|^{l+1}}=\frac{4\pi}{2l+1}\sum_{L'L''}D^L_{L'L''}\frac{a^{l'}}{b^{l''+1}}Y_{L'}(\hat{\mathbf{a}})Y_{L''}(\hat{b})\ , \tag{A18}$$

which attains the usual structure of harmonic functions. The coupling coefficient $D^L_{L'L''}$ essentially is the Gaunt coefficient with the additional selection rule $l''=l+l'$

$$D^L_{L'L''}=(-)^l\frac{(2l+1)l!(2l+l')!}{(2l)!(l+l')!2^{l'}(2l'+1)!!}\times C^L_{L',L''}\delta_{l'',l+l'}\ . \tag{A19}$$

From (A16) and (A18) the result previously introduced (18) is obtained directly with the expansion coefficient $\gamma^{\mu,\nu}_L$ given by

$$\gamma^{\mu,\nu}_L=\sum_{L'>0}\sum_{L''}\left[\frac{s_\mu}{a_{\mu\nu}}\right]^{l'+1}\left[\frac{s_\nu}{a_{\mu\nu}}\right]^l S^\mu_L(1)D^{L'}_{LL''}\beta^{\mu,\nu}_{L''} \tag{A20}$$

and the same radius of convergence as U_1. Finally, we want to mention that the sum over L in the second term of (18) also includes $L=(0,0)$, yielding a constant shift in the spherical symmetric potential.

[1]P. Hohenberg and W. Kohn, Phys. Rev. **136**, B864 (1964); W. Kohn and L. J. Sham, *ibid.* **140**, 1133 (1965); L. J. Sham and W. Kohn, *ibid.* **145**, 561 (1966).
[2]H. Bross, Phys. Kondens. Mater. **3**, 119 (1964); Helv. Phys. Acta **41**, 717 (1968); G. Bohn, G. Meister, W. Schubö, and H. Stöhr, Phys. Rev. B **2**, 3098 (1970).
[3]H. Bross and R. Eder, Phys. Status Solidi B **144**, 175 (1987).
[4]H. Bross and R. Stryzek, Phys. Status Solidi B **144**, 625 (1987).
[5]J. Callaway and C. S. Wang, Phys. Rev. B **7**, 1096 (1973); C. S. Wang and J. Callaway, *ibid.* **9**, 4897 (1974); J. Callaway and

L. J. Fry, in *Computational Methods in Band Theory,* edited by P. M. Marcus, J. F. Janak, and A. R. Williams (Plenum, New York, 1974); R. C. Chaney, T. K. Tung, C. C. Lin, and E. E. Lafont, J. Chem. Phys. **52**, 361 (1970).
[6]D. D. Koelling and G. O. Arbman, J. Phys. F **5**, 2041 (1975).
[7]O. K. Andersen, Phys. Rev. B **12**, 3060 (1975).
[8]D. R. Hamann, Phys. Rev. Lett. **42**, 662 (1979); E. Wimmer, H. Krakauer, M. Weinert, and A. J. Freeman, Phys. Rev. B **24**, 864 (1981); H. J. F. Jansen and A. J. Freeman, *ibid.* **30**, 561 (1984); S. H. Wei and H. Krakauer, Phys. Rev. Lett. **55**, 1200 (1985); S. H. Wei, H. Krakauer, and M. Weinert, Phys. Rev. B **32**, 7792 (1985).
[9]M. Weinert, E. Wimmer, and A. J. Freeman, Phys. Rev. B **26**, 4571 (1982).
[10]D. Singh, Phys. Rev. B **43**, 6388 (1991); D. Singh and H. Krakauer, *ibid.* **43**, 1441 (1991).
[11]L. F. Mattheiss and D. R. Hamann, Phys. Rev. B **33**, 823 (1986).
[12]H. Bross, O. Belhachemi, B. Mekki, and A. Seoud, J. Phys. Condens. Matter **2**, 3919 (1990).
[13]G. E. Engel and B. Farid, Phys. Rev. B **46**, 15 812 (1992).
[14]H. Bross and G. M. Fehrenbach, Z. Phys. B **81**, 233 (1990).
[15]L. Kleinman and R. Shurtleff, Phys. Rev. **188**, 1111 (1969).
[16]J. Molenaar, J. Phys. Condens. Matter **1**, 6559 (1989); E. Badralexe and A. J. Freeman, Phys. Rev. B **37**, 1067 (1988).
[17]F. Calogero, *Variable Phase Approach to Potential Scattering* (Academic, New York, 1967).
[18]H. Hämmerlin and K. H. Hoffmann, *Numerische Mathematik* (Springer, Berlin, 1989); J. S. Vandergraft, *Introduction to Numerical Computations* (Academic, Orlando, 1983); J. Stoer and R. Bulirsch, *Introduction to Numerical Analysis* (Springer, New York, 1980); C. de Boor, *A Practical Guide to Splines* (Springer, New York, 1978).
[19]J. Strang and G. J. Fix, *An Analysis of the Finite Element Method* (Prentice-Hall, Englewood Cliffs, NJ, 1973).
[20]V. L. Moruzzi, J. F. Janak, and A. R. Williams, *Calculated Electronic Properties of Metals* (Pergamon, New York, 1978).
[21]T. Takeda and J. Kübler, J. Phys. F **9**, 661 (1979).
[22]E. O. Condon and G. H. Shortley, *The Theory of Atomic Spectra* (Cambridge University Press, Cambridge, England, 1935); M. E. Rose, *Multipole Fields* (Wiley, New York, 1955).
[23]D. J. Chadi and M. L. Cohen, Phys. Rev. B **8**, 5747 (1973); D. J. Chadi, *ibid.* **16**, 1746 (1977).
[24]H. J. Monkhorst and J. D. Pack, Phys. Rev. B **13**, 5188 (1976).
[25]H. Bross, J. Phys. F **8**, 2631 (1978).
[26]R. P. Feynman, Phys. Rev. **56**, 340 (1939); H. Hellmann, *Einführung in die Quantenchemie* (Franz Deutike, Leipzig, 1937); W. Pauli, in *Handbuch der Physik,* edited by H. Geiger and K. Scheel (Springer-Verlag, Berlin, 1933), Vol. 24-1, p. 161.
[27]H. Bross, Z. Phys. **243**, 311 (1971); N. W. Dalton, J. Phys. C **3**, 1912 (1970).
[28]G. Gilat and L. J. Raubenheimer, Phys. Rev. **144**, 390 (1966); L. J. Raubenheimer and G. Gilat, *ibid.* **157**, 586 (1967); G. Gilat, Phys. Rev. B **26**, 2243 (1982).
[29]G. Lehmann and M. Taut, Phys. Status Solidi B **57**, 815 (1973); **54**, 469 (1972); O. Jepsen and O. K. Andersen, Solid State Commun. **9**, 1763 (1971).
[30]H. Bross, Phys. Status Solidi B **179**, 492 (1993).
[31]W. E. Rudge, Phys. Rev. **181**, 1020 (1968).
[32]J. Ihm, A. Zunger, and M. L. Cohen, J. Phys. C **12**, 4409 (1979).
[33]M. I. Chodorow, Phys. Rev. **55**, 675 (1939); G. A. Burdki, *ibid.* **129**, 138 (1964).
[34]J. F. Janak, A. R. Williams, and V. L. Moruzzi, Phys. Rev. B **6**, 4367 (1972); **11**, 1522 (1975).
[35]A. H. McDonald, J. M. Daams, S. H. Vosko, and D. D. Koelling, Phys. Rev. B **25**, 713 (1982).
[36]D. Bagayoko, D. G. Laurent, S. P. Singhal, and J. Callaway, Phys. Lett. **76A**, 187 (1980).
[37]M. Norman and D. D. Koelling, Phys. Rev. B **28**, 4357 (1983).
[38]H. Przybylski and G. Borstel, Solid State Commun. **52**, 713 (1984).
[39]L. Hedin and B. I. Lundqvist, J. Phys. C **4**, 2064 (1971).
[40]O. Gunnarson and B. I. Lundqvist, Phys. Rev. **13**, 4274 (1976).
[41]J. C. Slater, Phys. Rev. **51**, 846 (1937).
[42]L. D. Jennings, D. R. Chipman, and J. J. DeMarco, Phys. Rev. **135**, 1612 (1964).
[43]A. Freund, Ph.D. thesis, Technische Universität München, 1973.
[44]J. R. Schneider, N. K. Hanse, and H. Kretschmer, Acta Crystallogr. Sec. A **37**, 711 (1981).
[45]J. R. Temkin, V. E. Henrich, and P. M. Raccah, Phys. Rev. B **6**, 3572 (1972).
[46]J. H. Rose, J. Ferrante, and J. R. Smith, Phys. Rev. Lett. **47**, 675 (1981).
[47]*Handbook of Physics and Chemistry,* edited by R. C. Weast (CRC, Boca Raton, FL, 1983).
[48]W. C. Overton, Jr. and J. Gaffney, Phys. Rev. **98**, 969 (1955).
[49]J. B. Mann (unpublished). As cited in Table 1.1 of Ref. 20.
[50]U. Himmler, H. Peisl, A. Sepp, and W. Waidelich, Z. Angew. Phys. **28**, 104 (1969).
[51]K. A. Gschneidner, Jr., *Solid State Physics,* edited by F. Seitz and D. Turnbull (Springer, Berlin, 1964), Vol. 16, p. 276; Tables VII, XVI, and XXIV.
[52]P. Thiry, D. Chanderesis, J. Lecante, G. Guillot, A. Pinchaux, and Y. Petroff, Phys. Rev. Lett. **43**, 82 (1979).
[53]A. K. Rajagopal, in *Advances in Chemical Physics,* edited by G. I. Prigogine and S. A. Rice (Wiley, New York, 1979), Vol. 41.
[54]D. C. Langreth and M. J. Mehl, Phys. Rev. Lett. **47**, 446 (1981).
[55]J. P. Perdew, J. A. Chevary, S. H. Vosko, K. A. Jackson, M. R. Pederson, D. J. Singh, and C. Fiolhais, Phys. Rev. B **46**, 6671 (1992); J. P. Perdew, in *Electronic Structure of Solids '91,* edited by P. Ziesche and H. Eschrig (Akademie, Berlin, 1991).
[56]J. P. Perdew and W. Yue, Phys. Rev. B **33**, 8800 (1986); J. P. Perdew, Phys. Rev. Lett. **55**, 1665 (1985).
[57]L. Hedin, Phys. Rev. **139**, A796 (1965); L. Hedin and S. Lundqvist, *Solid State Physics,* edited by F. Seitz, D. Turnbull, and H. Ehrenreich (Springer, Berlin, 1969), Vol. 23, p. 1.
[58]M. Weinert, J. Math. Phys. **22**, 2433 (1981).
[59]P. P. Ewald, Ann. Phys. (Leipzig) **24**, 253 (1921); G. Leibfried, in *Hundbuch der Physik* XXIV 1, edited by S. Flügge (Springer, Berlin, 1955); J. M. Ziman, *Principles in the Theory of Solids* (Cambridge University Press, Cambridge, England, 1965).
[60]H. Bross (unpublished).
[61]J. D. Jackson, *Classical Electrodynamics* (Wiley, New York, 1965).
[62]*Handbook of Mathematical Functions,* edited by M. Abramowitz and I. A. Stegun (Dover, New York, 1965).
[63]A. R. Williams, S. M. Hu, and D. W. Jepsen, in *Computational Methods in Band Theory* (Ref. 5); A. R. Williams and J. van W. Morgan, J. Phys. C **7**, 37 (1974).